Research Articles

Competitive Scavenging of Trace Metals by HFO and HMO during Redox-driven Early Diagenesis of Ferromanganese Nodules

Dedicated to Prof. Dr. Ulrich Förstner on his 65th birthday

Michael Kersten[1]* and Dmitrii A. Kulik[2]

[1]Geoscience Institute, Gutenberg-University, D-55099 Mainz, Germany
[2]Waste Management Laboratory, Paul-Scherrer-Institute, CH-5232 Villigen-PSI, Switzerland

* **Corresponding author** (michael.kersten@uni-mainz.de)

DOI: http://dx.doi.org/10.1065/jss2005.02.130

Abstract

Background. Surface complexation models (SCM) alone have yet less successfully reproduced sorption isotherms of hydrous manganese oxides (HMO). This is in part due to the fact that the HMO structure may vary with pH, and also because microbially formed natural HMO has an oxidation number O/Mn < 2, i.e. is of non-stoichiometrical composition. The former effect has often led to severe artefacts, such as an underprediction of metal sequestration at low pH, and non-comparable pK and pH_{ZPC} values in literature. The latter effect is of particular importance for environments of varying redox conditions like sediments.

Objectives. We propose therefore a new sorption model comprising of amphoteric site SCM, ion exchange due to permanent charge compensation, and solid solution formation, in order to comply at least in part with the redox complexity of HMO phases of stable birnessite- and buserite-type structures.

Methods. The model is run by a new Gibbs energy minimization code which is shown to be particularly suitable for such a sorption continuum approach.

Results and Discussion. Initial calibration of the model was performed by experimental literature data on simple laboratory systems. Thus parameterised, we simulated on the basis of available field data the effect of redox-driven dissolution of a ferromanganese nodule on the partitioning of metals between the interacting HMO, HFO, and marine water phases. Our scenario model suggests that significant fraction of Mn and other metals, probably 50% or more, may be recycled to water column from the surface of the ferromanganese nodule upon gradual development of the bottom water stagnation, except of Zn for which a by far stronger net retention was found.

Conclusion and Outlook. Our model, even if only a first approximation, clearly shows that stagnation in the marine bottom water, once occurring, can drastically change primary element proxy records in ferromanganese nodules, smoothing out any anomalous patterns in the most recent record.

Keywords: Adsorption; Baltic Sea; early diagenesis; ferromanganese nodules; geochemical modeling; hydrous ferric oxides (HFO); hydrous manganese oxides (HMO); redox potential; sorption model; surface complexation models (SCM); trace metals

Introduction

Hydrous manganese oxides (HMO) are receiving increasing interest both in biogeochemistry, due to the importance of microbial catalysis in their formation, and in environmental geochemistry, due to their importance as trace metal sorbents in a wide number of environments. Accurate models of the mechanisms of trace metal sequestration not only in association with HMO, but also in competition with classical natural sorbents like hydrous ferric oxides (HFO), are thus required for an overall understanding of metal partitioning. Ferromanganese nodules are a classical HMO-bearing compound in sediments and soils, with accretion and metal scavenging time scales up to thousands of years. The implication that they provide a continuously growing substrate with invariable sorption efficiency for trace elements is the basis of a resuming interest for the nodules, focusing on their possible use as a paleoproxy record for long-term environmental changes. Detailed knowledge of chemical composition and accretion rates is necessary to construct models of the fluxes of these elements into the nodules. The first evidence for the potential of monitoring anthropogenic impact with these nodules was suggested for samples from sediments of the Baltic Sea, were trace metals were found to be enriched in the outermost layers (Glasby et al. 1997, Hlawatsch et al. 2002a).

Element maps of Fe and Mn show typically a cuspate alternating zebra-type band structure in these nodules (Glasby et al. 1997, Hlawatsch et al. 2002a, Marcus et al. 2004). The botryoidal onion-like growth pattern of alternating Fe- and Mn-rich layers has been attributed to cycling variations in bottom water conditions (Hlawatsch et al. 2002b). The outermost layers are richer in Fe and characterized by higher porosity which may reflect a recent period of enhanced bottom water stagnation and post-depositional partial re-dissolution of the HMO compound. The implication that the oxide layers provide a continuous growing and invariable scavenger for trace elements has therefore been questioned. More data are necessary on the 'invariable sorption efficiency' argument. Experimental and modeling data are yet sparse for understanding the impact of varying redox conditions on trace metal adsorption by mixed Mn/Fe-oxides. In this contribution, a sorption continuum modeling approach is suggested in order to explain (i) the effect of al-

ternating HFO/HMO substrate availability on competitive trace metal scavenging, (ii) the influence of consecutive redox-driven dissolution of the redox-sensitive HMO phase on trace metal release, and (iii) why the Zn concentration is typically increased in outer rims during early diagenesis, but not to that extend of Cu, Cd or other anthropogenic heavy metals (Hlawatsch et al. 2002a).

1 Geochemical Models

1.1 The Gibbs energy minimization approach

Processes of oxidative precipitation or reductive dissolution of oxides are microbially controlled and occur in most cases rather rapidly. Thermodynamic equilibrium models are therefore justified as a suitable tool in understanding and interpretation of the field data. In principle, there are two methods of thermodynamic speciation modeling which can be applied to such complex early-diagenetic systems: (i) Law-of-Mass-Action – Reaction Stoichiometry (LMA-RS), and (ii) Gibbs Energy Minimization (GEM). The LMA-RS approach is commonly available in many computer codes such as PHREEQC. It requires no thermodynamic data for components (usually aqueous ions) but only logK of formation of species derived from the components by a stoichiometric matrix of independent reactions. However, this leads to serious limitations in setting up more complex geochemical models in that (i) stable phase association must be known *a priori* to be included into the mass balance, (ii) compositions of aqueous and solid solution phases at equilibrium can not be directly solved but one of them must be fixed as input, (iii) surface complexes are treated similar to aqueous complexes, without any link to the stability of their solid phase carrier, but with an additional mole balance constraint for each surface site type, and last but not least (iv) different redox states of the same element, e.g., Fe^{2+} and Fe^{3+}, must be assigned to separate mass-balance constraints, with an additional equation defining the ambient redox potential.

Gibbs energy minimization (GEM) codes have been developed in parallel with LMA-RS codes, but are relatively uncommon in low temperature geochemical modeling because of higher demand for consistency in the thermodynamic database. GEM was already applied with success for modeling major element speciation, alkalinity, and redox conditions in the Baltic Sea (Kulik and Harff 1993), and more recently also for sorption continuum models comprising both of multi-site multi-surface adsorption and ion exchange on single- or solid-solution sorbents (Kulik 2000, 2002a,b). The GEM approach is based, in principle, on a mass balance in any chemical system which is set up using total quantities of chemical elements and a single charge balance constraint, without distinction between component and product species. For each species which may appear at equilibrium state, the formula stoichiometry and a value of (partial molar/molal) Gibbs energy of formation from elements must be provided at the respective temperature and pressure from the thermodynamic database. Chemical potentials of all elements are calculated at equilibrium. On this basis, a stable phase assemblage from any number of possible phases is automatically selected and leads directly to solution of the speciation problem in any number of coexisting (non-ideal) solid, liquid, aqueous, gaseous and/or sorbate phases. Quantities of surface species are automatically normalized according to the current stable quantity of the adsorbent phase, surface charge/potential, and limiting surface site density. Therefore no additional balance constraints are required, and surface precipitation can also be reproduced in parallel. Our GEM approach originally encoded in the program Selektor-A (now superceded by the GEMS-PSI program package: http://les.web.psi.ch/Software/GEMS-PSI/) can always find equilibrium values of pH, pe (Eh), and partial pressures of gases from bulk composition of the aquatic system, and can also automatically detect inconsistencies in the thermodynamic data input (Karpov et al. 1997, Kersten and Kulik 2005).

The aqueous ion-association model used in this study (Kulik and Harff 1993, Kulik et al., 2000) considers the main interactions of all solid phases with aqueous solutions and dissolved gases, forming the stoichiometry matrix of more than 700 chemical species for the whole elemental system (B-Ca-N-C-S-Cl-Br-F-K-Mg-Na-Sr-P-Si-Al-Fe-Mn-O-H-*Nit*-Zn-Cd-Cu-Ni-*e*-*Cit*). Thermodynamic data including standard partial molal properties of aqueous species are derived from the equation-of-state correlation approach (Shock et al. 1997, Sverjensky et al. 1997). The citrate ligand represents all natural organic complexants for aqueous cations. No attempt was made to include one of the more sophisticated multi-ligand complexation or non-specific binding models, due mainly to a lack of relevant analytical data on the forms and molecular properties of marine dissolved organic matter (DOM). The three-term extended Debye-Hückel equation with Kielland ion-size parameters and common third parameter $b_\gamma = 0.064$ was used to calculate activity coefficients for aqueous ions and complexes; a detailed compilation for major dissolved ions used for the normative Baltic Sea water phase was given by Kulik and Harff (1993). Since the carbonate system plays a key role in accurate modeling of sea water geochemistry, the thermal dependence of the $NaHCO_3^0$ complex was fine-tuned for precise calculation of carbonate system parameters (pH, fCO_2, alkalinity A_C) at ambient Baltic Sea water salinity, temperature, and pressure. Note also that gaseous nitrogen has been decoupled from the nutrient nitrogen species (NO_3, NH_3, etc.). To reduce modeling errors at temperatures below 25°C, standard values of molar enthalpy H^0, entropy S^0, and heat capacity Cp^0 were taken from available literature where possible, otherwise estimated (Kersten and Kulik 2005).

1.2 Setup of the adsorption models

The trace metal adsorption models for both the HFO and HMO sorbent differ in that a conventional one was used for the former, while a new redox-dependent one is introduced for the latter.

1.2.1 The HFO sorbent

The HFO phase of the ferromanganese nodules in the western Baltic Sea is composed of 2-line ferrihydrite (Hlawatsch et al. 2002b, Marcus et al. 2004). The yet most commonly accepted compilation of adsorption model data for HFO

Table 1: Thermodynamic data for the HFO sorbent phase

Species	pK^{int} (DM90)[a]	pK^0, this work	g^0_{298}, kJ·mol^{-1}	Stoichiometry for GEM
$\equiv OCu^+_s$	–2.89	–0.45	–65.532	$O_{0.5}Cu^+$
$\equiv ONi^+_s$	–0.37	2.07	–162.338	$O_{0.5}Ni^+$
$\equiv OCd^+_w$	2.90	3.82	–184.399	$O_{0.5}Cd^+$
$\equiv OCd^+_s$	–0.47	1.97	–194.958	$O_{0.5}Cd^+$
$\equiv OZn^+_w$	1.99	2.83	–259.671	$O_{0.5}Zn^+$
$\equiv OZn^+_s$	–0.99	1.46	–267.491	$O_{0.5}Zn^+$
$\equiv OMn^+_w$	3.50[b]	4.42	–333.857	$O_{0.5}Mn^+$
$\equiv OMn^+_s$	0.40[b]	2.84	–342.875	$O_{0.5}Mn^+$
$\equiv OCa^+_w$	5.85	6.77	–642.695	$O_{0.5}Ca^+$
$\equiv OHBa^{+2}_s$	–5.46	–3.02	–706.568	$O_{0.5}HBa^{+2}$
$\equiv OSr^+_w$	6.58	7.50	–649.574	$O_{0.5}Sr^+$
$\equiv OHSr^{+2}_s$	–5.01	–2.57	–707.053	$O_{0.5}HSr^{+2}$
$\equiv H_2PO_4^0$	31.29	30.37	–1202.107	$H_3PO_4^0$
$\equiv HPO_4^-$	25.39	24.47	–1168.430	$H_2PO_4^-$
$\equiv PO_4^{-2}$	17.72	16.80	–1124.650	HPO_4^{-2}
$\equiv H_2BO_3^0$	–0.52	0.30	–977.007	$H_3BO_3^0$
$\equiv OHSO_4^{-2}$	–0.79	0.13	–872.265	$O_{0.5}HSO_4^{-2}$
$\equiv OH_2^+$	7.29	6.45	–165.364	$O_{0.5}H_2^+$
$\equiv O^-$	8.93	9.77	–72.781	$O_{0.5}^-$
$\equiv OH^0$	–	–	–128.55[c]	$O_{0.5}H^{0c}$
HFO	–	–	–558.748[d]	FeOOH

[a]data from compilation by Dzombak and Morel (1990)
[b]estimated from LFER (Fortin et al. 1993)
[c]Kulik (2002)
[d]recalculated from Melnik (1986) and corrected for variation in specific surface area *A* by adding an amount of 0.2933*A* (in J/mol, *A* in m^2/mol)

(Dzombak and Morel 1990) has been adopted into our thermodynamic database. Any intercalation of trace metals in the HFO structure was neglected. The intrinsic adsorption constants for the double layer model (DLM), valid at total surface site density of 3.84 µmol m^{-2} (2.31 sites nm^{-2}), were converted to thermodynamic adsorption constants and Gibbs energies of formation from elements using a standard site density of 20 µmol m^{-2} (Kulik 2000). The 'strong' and 'weak' sites for Zn and other metals on HFO were each assigned to a single surface type, but with different maximum site densities, Γ_{max}, and modes of calculation of 'surface activity terms' necessary for GEM modeling (Kulik 2000) as compiled in **Table 1**. A non-competitive surface activity term (SAT) with a Γ_{max} = 0.056 nm^{-2} was applied to the strong sorbent site density (e.g., $\equiv O_{0.5}Zn^+_s$, and other strong complexes), and a competitive SAT at Γ_{max} = 2.254 nm^{-2} to the weak site density (e.g., $\equiv O_{0.5}Zn^+_w$, and all remaining surface species except the neutral hydroxyl group $\equiv OH^0$, Kulik 2000).

1.2.2 The HMO sorbent

The HMO phase in the Baltic Sea ferromanganese nodules is a phyllomanganate with hexagonal layer symmetry of birnessite-type. Mn K-edge X-ray absorption spectroscopy (XAS) revealed that this disordered ('turbostratic') HMO phase contains about 9 mol-% of Mn^{3+} in octahedral layer positions, and no significant contribution of Mn^{2+} or Mn^{3+} in interlayer positions (Marcus et al. 2004). From initial theoretical reasoning, redox controlled changes in the Mn^{3+}/Mn^{4+} ratio of HMO phases would lead to significant changes in its adsorption properties even at constant solid particle concentration. This is because surface sites on Mn^{4+} would display acid-base behaviour similar to that found on SiO_2 or TiO_2, with rather low point of zero charge (pH_{pzc}), whereas surface sites on Mn^{3+} are expected to behave similar to those on other oxides of trivalent metals, e.g. ferrihydrite, goethite, alumina, with much higher pH_{pzc} values. Under neutral conditions (pH = 7), reduction of the system alone may lead at least to an inversion of the surface electric potential on HMO from negative to neutral and even positive charge, if not followed by an irreversible structural transformation.

For proceeding with thermodynamic description of mixed-valent HMO phases, an initial albeit reliable approximation is that reduction of the oxidation number (O/Mn ratio) occurs without net release of Mn into aqueous solution, but rather results in structural intercalation of Mn^{3+} ions. From a thermodynamic point of view, the new phase can at least formally be expressed as a solid solution of composition $(MnO_2)_{2n-3}(MnOOH)_{4-2n}$, at least for the natural oxidation

number range 1.5 < n < 2.0 (Tye 1985, Gramm-Osipov et al. 1989). It follows that at fixed pH, pe, and Mn^{+2} ion activity in aqueous solution, only one composition, with fixed n value, of the non-stoichiometric HMO is possible in thermodynamic solid solution – aqueous solution (SSAS) equilibrium. If redox conditions in the system change, this composition could change according to the disproportionation reaction:

$$2MnOOH + 2H^{+} = MnO_2 + 2H_2O + Mn^{+2} \quad (1)$$

This behaviour was experimentally confirmed at least for the transition of γ-MnO_2 (nsutite) to δ-MnOOH (Gramm-Osipov et al. 1992). Qualitatively this model should be applicable to other HMO end-member phases as well, but solubility studies along the reduction pathway from synthetic (hexagonal) birnessite to the respective γ-MnOOH end-member are yet to be performed. As long as no solubility data are available for this manganate series, a reliable approximation with respect to our thermodynamic HMO solid-solution model is to assume the ideal mixing behaviour of the end-members (**Table 2**).

Table 2: Thermodynamic data for the HMO phase

End–members	g^0_{298}, kJ mol^{-1}	Reference
MnO_2	–459.74[a]	Kulik and Kersten (1998)
MnOOH	–567.09[a]	Kulik and Kersten (1998)
$\equiv O_{0.5}H^0$ (SOH^0)	–128.55	Kulik (2002)

[a]includes stability correction of +10.04 kJ mol^{-1} for the specific surface area

For the mechanism of bivalent trace metal cation sorption by HMO, molecular level XAS analysis of a ferromanganese nodule sample indicates that the tetrahedrally coordinated Zn is not substituting for structural Mn. The metal cation is rather sorbed as interlayer tridentate corner-sharing surface complex for compensation of the permanent charge deficiency originating both from replacement of Mn^{4+} by Mn^{3+}, and by formation of vacancies in the structural layer not fully compensated for by interlayer (also corner-sharing) Mn^{3+} octahedra (Marcus et al. 2004). We may attribute the pool of active sorption sites in interlayer positions capping the vacant layer octahedra to a formal permanent charge cation exchange capacity in (non-structural) analogy to phyllosilicates (CEC, Tanaka and Tsuji 1997). In order to account for cation sorption in the interlayer, we therefore introduced an ion exchange model. Birnessite- and buserite-type HMO phases (with oxidation numbers ≈ 1.7–1.9) show the highest possible formal CEC of up to 0.3 mol per mol Mn (Manceau et al. 2002). At a marine water pH = 8.1, the permanent-charge 'X-sites' are completely occupied by ion exchange with Na^{+} and other cations. From a thermodynamic point of view, we could now suppose that formal CEC values are determined by the mole fraction of the Mn^{3+} end-member MnOOH (9% in our case), and thus would decrease towards the MnO_2 end-member composition. At an assumed specific surface of 300 m^2 g^{-1} for the HMO phase, this results in a maximum formal CEC of about 680 µmol g^{-1} at charge density of = 4.7 sites nm^{-2}, or 7.8 µmol m^{-2} for the ion-exchange 'X-type' sites.

At the outer 'edge' surface of the particles, a diffuse double layer may exist which may contribute to the sorption capacity, in particular of colloidal sized turbostratic birnessites. These remaining surface sites are thought to be occupied by various amphoteric hydroxyl groups just again as in case of clay minerals, which were accounted for by a conventional 2-pK triple layer surface complexation model (TLM). Macroscopic metal adsorption studies have shown strong solution-concentration and pH effects manifested in a large scatter of the effective pK_{ads} values (Tonkin et al. 2004). This might be due to the fact that surface complexation modeling of sorption isotherms as a function of pH has no structural foundation because the HMO structure varies with pH as mentioned above, and discussed in more detail by Manceau et al. (2002). On the other hand, we may keep for a first approximation up with the still common assumption that the changing HMO surface may act like a heterogeneous sorbent, for which single-site models are inadequate (Appelo and Postma 1999). We assume that the interlayer X-site exchange groups discussed above cover 1/3 of the total available surface, while the weak outer- and inner-sphere (TLM type 1) amphoteric hydroxyl groups cover the remainder 2/3 of the total available surface area (Γ_{Me} > 30 mmol per mol Mn).

In addition, weak adsorption of trace metals may become relevant at a higher dissolved metal pool (Me_{aq} > 1 µmol L^{-1}). These weak surface sites may be represented by outer-sphere (OS) complexes as suggested by XAS data of respective experimental systems (Trivedi et al. 2001). Strong amphoteric sites at hydroxyl surface groups govern inner-sphere (IS) metal cation adsorption at Γ_{Me}< 1 mmol per mol Mn, and may keep the dissolved trace metal pool at Me_{aq} < 1 nmol L^{-1}. This site heterogeneity is accounted for by adding double-coordinated, 2 pK units stronger inner-sphere sites of TLM-type 2 but allocated to only 1% of the surface area at standard site density. Introduction of very strong, selective tridentate complex above vacant Mn in the outermost octahedral layer may explain high binding constants ('di-protic inner-sphere complexation': Appelo and Postma 1999). However, these sites may represent at most only a small proportion of surface complexes (Γ_{Me} < 30 µmol per mol Mn) necessary to account for metal adsorption at low outer surface coverage (< 0.1%). We assume that these TLM-type 3 surface sites form at a very low density of less than 0.03 sites nm^{-2}, with 3.5 pK units stronger than TLM-type 1 site. All amphoteric surface types are assumed to develop their own surface charge potential due to inner- and outer-sphere surface complexation, as described by the TLM model types and the parameters listed in **Table 3**. Thermodynamic properties of additional monodentate ternary X-MeL^0 and >$OMeL_X$ surface complexes (with L = OH^- or Cl^-) typical for high ionic strength marine waters were adjusted simultaneously for all surface types, based on a LFER correlation with stability of respective aqueous chloro- and hydroxo complexes. Note, however, that the model is more sensitive to area fractions occupied by the various surface types given by the structural data, and to Γ_{max} of strong sites, than to particular values of pK_{ads}. Separate SCM for the MnOOH end-member has not been considered, since Zn has been found by XAS to form surface precipitates rather than significant amount of (inner-sphere) surface complexes on this phase (Bochatay and Persson 2000).

Table 3: Parameters used in the HMO adsorption model

Parameter, species	Symbol	Value	Comments
Specific surface area	A	290 $m^2\ g^{-1}$	C&L86[a]
TLM1 surface type	ϕ_1	0.69	At $\Gamma_{max} = \Gamma^0$
TLM2 surface type	ϕ_2	0.01	At $\Gamma_{max} = \Gamma^0$
X surface type	ϕ_X	0.30	Γ_{max} adjusted
TLM outer capacitance	C_2	0.2 F m^{-2}	Common for TLM
TLM1 inner capacitance	$C_{1,1}$	2.4 F m^{-2}	From C&L86[a]
TLM2 inner capacitance	$C_{1,2}$	1.2 F m^{-2}	Assumed
TLM1,2 $\equiv O_{0.5}H_2^+$ $\equiv O_{0.5}^-$ $\equiv O_{0.5}^-Na^+$	pK^0_{a1} pK^0_{a2} pK^0_{Na}	1.6 8.0 4.7	At pH_{PPZC} = 4.8 as for γ–MnO_2; same ΔpK_a as predicted for TiO_2 (S&S96[b]) Equation 2, θ = 3.0
TLM1 $\equiv O_{0.5}^-Zn^{+2}$ $\equiv O_{0.5}^-ZnOH^+$	$pK^0_{Zn,OS}$ $pK^0_{ZnOH^+}$	1.3 9.3	Predicted, θ = 3.0 Predicted, θ = 3.0
Γ_{max} of X surface	Γ_X	7.8 µmol m^{-2}	Fitted using data by C&L86[a]

[a]Catts and Langmuir 1986
[b]Sverjensky and Sahai 1996

This complex SCM has been parameterized against a classical experimental data set reported on Zn adsorption by a birnessite-type HMO (Catts and Langmuir 1986). The combined exchange and surface complexation model was used to calculate the amount of adsorbed Zn at varying pH. The result shows a nearly perfect match with the experimental data even in the low pH region, and at increased solid concentrations, for which under-prediction by conventional surface complexation modeling was commonly found (**Fig. 1**). The model was thereby shown to be sensitive to (i) area fractions of surface types (ϕ) in all cases, (ii) Γ_{max} for ion exchange X-sites at high dissolved metal species Me_{aq}, and for strong TLM-2,3 sites at low Me_{aq}, (iii) pK^0 of TLM-1,2,3 IS sites at I > 0.1 and/or at lower solid concentrations, (iv) pK^0 of

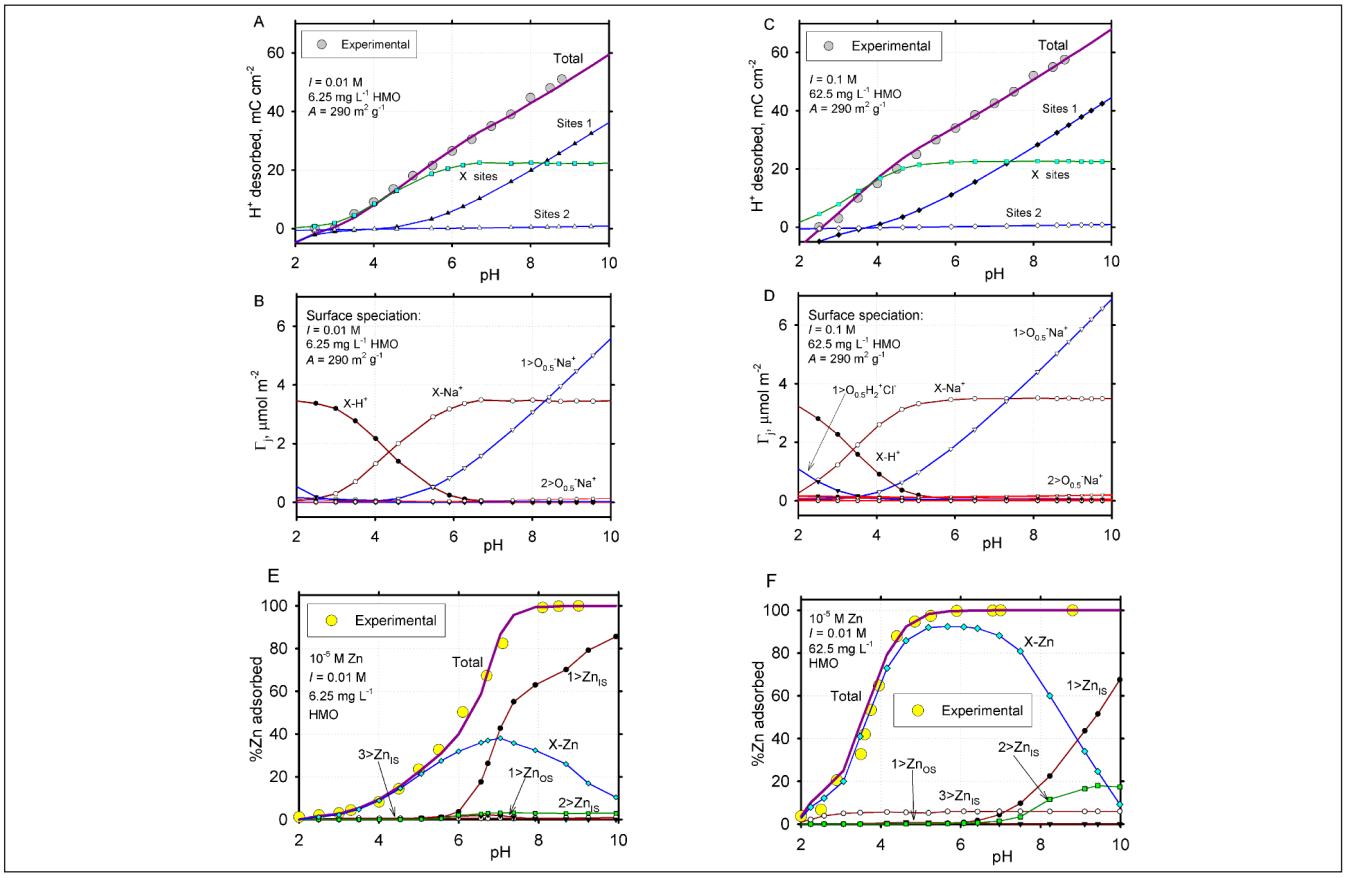

Fig. 1: Modelled surface deprotonation (A, B in 0.01 M NaCl onto 6.75 mg L^{-1} HMO; C,D in 0.1 M NaCl onto 67.5 mg L^{-1} HMO), and Zn (10 µM total) adsorption pH edges in 0.01 M NaCl (E onto 6.75 mg L^{-1} HMO; F onto 67.5 mg L^{-1} HMO), both compared to the batch experiment data (open circles) from Catts and Langmuir (1986). HMO specific surface area A = 290 $m^2\ g^{-1}$. Surface site types: 1 – TLM with C1 = 2.4 F m^{-2} occupying 67% of HMO surface; 2 – TLM with C1 = 1.2 F m^{-2} occupying 3% of HMO surface; X – NEM occupying 30% of HMO surface. For other model parameters, see text and Tables 3 and 4

exchangeable metal species X-Me^{+2} species at I < 0.1 and pH < 6, (v) pK^0 of ternary X-MeL^+ species (represented here by X-$MeOH^+$) at pH > 6, especially at relatively high X_{HMO} content, but (vi) insensitive to pK^0 of outer-sphere metal species. The resulting TLM parameters are given in Table 3.

In this parameterisation exercise, potential correlations were exploited in order to (i) reduce the number of adjustable parameters, and (ii) predict adsorption constants for other metals not covered by experimental data (Catts and Langmuir 1986). For the latter, we assumed that at each amphoteric surface site type, the differences between the inner- and outer-sphere adsorption constants pK^0_{Me+2}, pK^0_{MeOH+}, and $pK^0_{Me(OH)2}$, respectively, for a given metal are proportional to differences in the respective aqueous hydrolysis equilibrium constants (LFER correlation assumption according to Tessier et al. 1996). In fitting metal adsorption data by GEM-TLM, the respective adsorption constant values were varied simultaneously by adjusting the θ parameter in an equation introduced by Smith and Jenne (1991):

$$pK^0_{>M(OH)_n^{(2-n)+}} = pK^0_{A2} - \theta - \vartheta \log \beta_{1n} - 0.1\left[g_1\left(\frac{z}{r^2} + g_2\right)\right] \quad (2)$$

where $\vartheta = 0.86$, and g_1, g_2, r, and z refer to the Brown-Sylva-Ellis equation (Brown et al. 1985). Values of θ for all cations are assumed the same on a given TLM-type site for HMO. The θ values for TLM-1 and TLM-2 sites were obtained from Zn fits (**Table 4**). For ion-exchange X-sites, the relative pK_{Me} differences were estimated from data on bivalent cation release from buserite-type phyllomanganates (Giovanoli et al. 1975). For X-$MeOH^+$ species, pK difference from X-$Me_{0.5}^+$ was taken the same as for Zn. The thus obtained set of interim thermodynamic adsorption constants is presented in **Table 5**. For GEM calculations, these constants can now be converted to values of partial molal Gibbs energy g^0_{298} at standard site density, consistent to that for aqueous ions from SUPCRT database (Shock et al. 1997), using a $g^0_{298}(\equiv O_{0.5}H^0) = -128.55$ kJ mol^{-1}, and respective stoichiometric formulations for the

ion exchange site X:

$$X\text{-}H^+ + 0.5Me^{+2} = X\text{-}Me_{0.5}^+ + H^+ \quad (3a)$$

$$X\text{-}H^+ + MeOH^+ = X\text{-}MeOH^+ + H^+ \quad (3b)$$

outer-sphere surface complex site OS:

$$\equiv O_{0.5}H^0 + Me^{+2} = >O_{0.5}^-Me^{+2} + H^+ \quad (4a)$$

$$\equiv O_{0.5}H^0 + H_2O + Me^{+2} = >O_{0.5}^-MeOH^+ + 2H^+ \quad (4b)$$

and inner-sphere surface complex site IS:

$$\equiv O_{0.5}H^0 + Me^{+2} = >O_{0.5}Me^+ + H^+ \quad (5a)$$

$$\equiv O_{0.5}H^0 + H_2O + Me^{+2} = >O_{0.5}MeOH^0 + 2H^+ \quad (5b)$$

$$\equiv O_{0.5}H^0 + 2H_2O + Me^{+2} = >O_{0.5}Me(OH)_2^- + 3H^+ \quad (5c)$$

Table 4: Surface species used in the HMO adsorbent model

Model	Species	Symbol	Value (μmol m^{-2})	Comments
X	X-H^+	pK^0_{XH+}	–8.3	All X-sites must be occupied at pH > 2
NEM	X-Na^+	$pK^0_{XH\text{-}Na}$	3.0	Fitted on C&L86 data
	X-$Zn_{0.5}^+$	$pK^0_{2XH\text{-}Zn}$	1.7	
	X-$ZnOH^+$	$pK^0_{XH\text{-}ZnOH}$	–3.5	
TLM1-IS	$\equiv O_{0.5}Zn^+$	pK^0_{OZn+}	2.4	Fitted on C&L86[a] data
	$\equiv O_{0.5}ZnOH^0$	pK^0_{OZnOH0}	10.4	equation 2, θ = 1.9
	$\equiv O_{0.5}Zn(OH)_2^-$	$pK^0_{Zn(OH)2-}$	15.9	equation 2, θ = 1.9
TLM3-IS	$3\equiv O_{0.5}Zn^+$	$pK^0_{3\equiv OZn+}$	–1.1	Assumed pK^0_{OZn+} - 3.5
TLM2	$\equiv O_{0.5}Zn^+$	pK^0_{OZn+}	0.4	Assumed pK^0_{OZn+} - 2.0
	$\equiv O_{0.5}ZnOH^0$	pK^0_{OZnOH0}	8.4	equation 2, θ = 3.9
	$\equiv O_{0.5}Zn(OH)_2^-$	$pK^0_{Zn(OH)2^-}$	13.9	equation 2, θ = 3.9

[a] Catts and Langmuir 1986

Table 5: Predicted GEM-TLM model constants for trace metal adsorption by HMO

Adsorbed species	X-site $pK_{H\text{-}Me}$	Outer-sphere pK^0 for TLM1 sites (θ = 3.0)	Inner-sphere pK^0 for TLM1 sites (θ = 1.9)	Inner-sphere pK^0 for TLM2 sites (θ = 3.9)	Strong type-3 pK^0 on TLM1 (θ = 5.4)
Mg^{+2}	2.5	3.25			
$MgOH^+$	–2.7	13.4			
Ca^{+2}	2.8	4.0			
$CaOH^+$	–2.4	15.1			
Cd^{+2}	1.5	1.7	2.8	0.8	–0.7
$CdOH^+$	–3.7	10.25	11.4	9.4	
$Cd(OH)_2^0$			20.3	18.3	
Cu^{+2}	1.1	0.05	1.14	–0.86	–2.36
$CuOH^+$	–4.1	6.6	7.7	5.7	
$Cu(OH)_2^0$			14.3	12.3	
Ni^{+2}	1.9	1.9	3.0	1.0	–0.5
$NiOH^+$	–3.3	10.4	11.5	9.5	
$Ni(OH)_2^0$			20.4	18.4	

2 Results and Discussion

Sorbent competition effects were first demonstrated for a simple laboratory batch titration system. For the more advanced Baltic Sea scenario modeling, two situations are deemed to be important in the deposition of ferromanganese nodules (Hlawatsch et al. 2002b): (i) summer stagnation below the thermocline, anoxia in the near-bottom fluffy layer, benthic release of dissolved Mn, Fe, Zn, P, and other redox-sensitive elements, and possible partial reductive dissolution of the nodule surface; and (ii) mixing of the water column in the fall due to break-up of the thermocline, causing oxidation of dissolved Mn^{2+} (and possibly also Fe^{2+}) and precipitation of particulate HMO (and HFO). A geochemical model should account at least for main trends in trace metal partitioning during these two major environmental settings.

2.1 Sorbent competition in a laboratory model system

Preliminary calculations performed with Selektor-A GEM code on the geochemical nodule system included calcite, HFO, and the ideal solid-solution HMO phase for the solid phases, 2pK TLM adsorption model of Mn^{2+} and Zn^{2+} on HMO, and DDL adsorption model of both cations onto HFO. Development of an anoxic conditions was simulated by titration of the system by DOM, where increasing organic carbon oxidation leads to reduced pO_2 just as in nature. The modeling results demonstrate quantitatively the competitive adsorption behaviour of Zn on both oxide phases in a pH range typically encountered at the sediment-water interface (see Table 1 and **Fig. 2a**). With respect to redox behaviour, increasing organic carbon oxidation in the model system, and thereby reduced pO_2, leads to nano-molal concentrations of dissolved Fe remaining practically constant at all Eh > 0 values, whereas dissolved Mn increases by several orders of magnitude. The oxidation number O/Mn decreases simultaneously from 1.99 to 1.5, followed by dissolution of the HMO phase, and repartitioning of Zn to the remaining scavenger.

2.2 Sorbent competition in a natural oxic model system

Harms (1996) found that 4 µmol L^{-1} of total dissolved Mn, and 0.4 µmol L^{-1} Fe, was accumulated in September 1993 in a 1 m thick near-bottom water layer over C_{org}-rich mud in Mecklenburg Bay, SW Baltic Sea. Upon storm-induced mixing of the water column in October, both Mn and Fe were found to be oxidized into particulate hydroxides. The dissolved heavy metal pool at the end of stagnation in the near-bottom water can be assessed from the available field data as listed in **Table 6**. The second mixing-precipitation event (Stage 2 in the above mentioned scenario) was modelled at a salinity of 22 ‰, temperature 5°C, pressure 1 bar, with 30 µmol total Fe+Mn in the system but at various Mn/Fe ratios, and excess of O_2 up to atmospheric saturation. Three times larger specific surface areas than the 200 m^2 g^{-1} used for HFO, and 90 m^2 g^{-1} for HMO, respectively, were reported from laboratory experiments (Dzombak and Morel 1990, Catts and Langmuir 1986), but even lower values were found in field (50 m^2 g^{-1} for HMO from the Gotland Deep of central Baltic Sea: Müller and Duffek 2001).

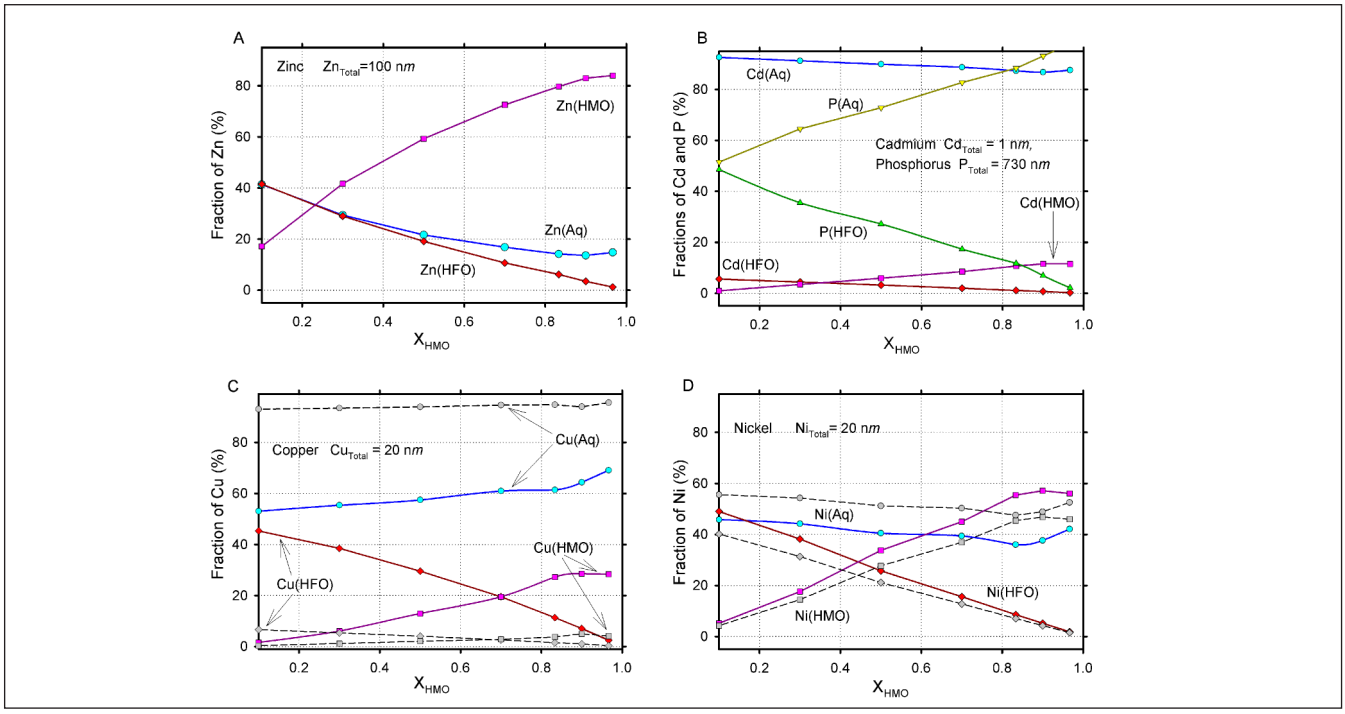

Fig. 2: Diagrams showing the partitioning of trace elements between HMO (total adsorbed), HFO (total adsorbed), and aqueous solution (total dissolved) as function of $X_{HMO} = n_{HMO}/(n_{HMO} + n_{HFO})$, where n_{HMO} is the variable amount of HMO (in µM) at constant sum $n_{HFO} + n_{HMO}$ = 30 µM. Symbols indicate model calculations, lines are guides for the eye. Dashed lines on graphs C and D correspond to a model variant in which the citrate complexation constants of Ca, Mg and Na have been made 30 times weaker.

Table 6: Field and model parameters for the sorbent dissolution and competitive scavenging scenario model

Parameter	Measured (Harms 1996)	Used for the model (total conc.)	Comments
Mn, µM	4	3–30	In the model, 30 µmol was taken for total diss. Mn+Fe
Fe, µM	0.4	1–30	
Cd, nM	0.4	1	
Cu, nM	87.5	20	
Ni, nM	21.6	20	
Zn, nM	80–100[a]	100	[a]Hlawatsch et al. (2002a)
P, µM	0.7–1.2	0.73	Average
DOC mg L^{-1}	2.2–3.3	10 µM	Citrate taken as ligand
T °C	5–15	5	Assumed for the fall season
$O_{2,aq}$, µM	4.9–33.4	400	Saturation state
S_B, g kg^{-1}	22	22	
BNSW, g kg^{-1}		21.935	Baltic Normative Sea Water model (Kulik and Harff 1993)
BNRW, g kg^{-1}		0.065	Baltic Normative River Water model (Kulik and Harff 1993)
Water, kg		978	Volumetric GEM model basis

Typical mean Mn/Fe ratio in nodule samples from the Mecklenburg Bay is 0.6 ± 0.1 (Hlawatsch et al. 2002a), which recalculated into the Mn mole fraction yields X_{HMO} = Mn/(Mn+Fe) = 0.62 ± 0.1. This is distinctly below the total dissolved Mn fraction in the near-bottom water ($X_{Mn,aq}$ = 0.91; Harms 1996), and may suggest that, on average, at least 30% of initially precipitated Mn gets re-mobilized upon formation of the nodules. The extent of such remobilization along the growth direction is highly variable, and may reach 70–80% or even more. Some layers may retain the same X_{HMO} as during precipitation, while others appear to be somewhat enriched in Mn. It is difficult to assess how $X_{Mn,aq}$ could vary with time, so precipitation of particulate Mn and Fe oxides was modelled at different bulk Mn/Fe ratios. Fig. 2 shows the modeling results in the form of graphs showing a percentage of adsorbed metals vs. $X_{Mn,aq}$ varying from 0.1 to 0.97. Cd and Cu are only weakly adsorbed (less than 20%), Ni is adsorbed at a level of ca. 40% regardless of the Mn/Fe ratio, but Zn is adsorbed up to 60–80%. At a X_{HMO} above 0.5, all metals are mainly adsorbed on HMO.

Cd and Zn are practically unaffected by the model organic (citrate) complexation, Ni is affected to some extent, but Cu is strongly affected. The preliminary calculations showed that up to 95% of citrate was bound to Ca, Na, and especially Mg. This is not the likely case for the natural dissolved organic matter, which is thought to be a complexant more specific for transitional metals than for first and second group elements. Hence, the stability of $CaCit^-$ and $NaCit^{-2}$ complexes was suppressed by 1.5 and that of $MgCit^-$ by even 2 pK units (30 and 100 times, respectively). This change in organic complexation affects Ni sorption to only about 10%, while plots for Zn and Cd were not at all affected (see Fig. 2). Clearly, Cu now is even more strongly complexed and adsorbs only weakly even at relatively high dissolved Cu and adsorbent concentrations, in agreement with what is known from voltammetric measurements in field (Hlawatsch et al. 2002b). Cadmium is weakly adsorbed because of the low inventory and strong inorganic complexation. It should be pointed out that the adsorption trends shown in Fig. 2 are non-linear, most probably due to surface heterogeneity of both phases reflected to some extent in our advanced adsorption model.

2.3 Natural model scenario with reductive HMO sorbent dissolution under anoxic conditions

An advanced modeling of the diagenetic ferromanganese nodule transformation requires considering of stagnation and reductive dissolution of at least some outer layer(s). For such an aqueous redox system (Stage 1 in the above mentioned scenario), we used the same bulk compositions of HMO and HFO phases as obtained from the previous modeling exercise (Stage 2), but now at a X_{HFO} = 0.9, corresponding to the field data for the near-bottom fluffy layer (Hlawatsch et al. 2002b). The most uncertain parameter in this stage is the effective solid/water ratio necessary for the GEM model setup. We can only speculate that this ratio within a thin fluffy layer in the nodule environment should be much higher than that chosen for the above formation stage (initial deposition of particulate Mn and Fe in the water column). We tried several ratios and found that any (Fe+Mn) > 1 mM produces unrealistically high dissolved Mn concentration and pH values (up to 8.5). Therefore, a reduced initial concentration of (Fe+Mn) = 300 µM was selected. O_2 reduction in the system was forced again by adding organic carbon (C_T) to the closed system. The effects of extensive reductive dissolution of the primary HMO precipitate on surface of the crust can be modelled at first approximation by assuming complete dissolution of HMO, while HFO remains unaffected ($Fe_{aq} \leq$ 0.1–0.2 nM). This would result in a quite high dissolved Mn = 270 µM, which, together with the released

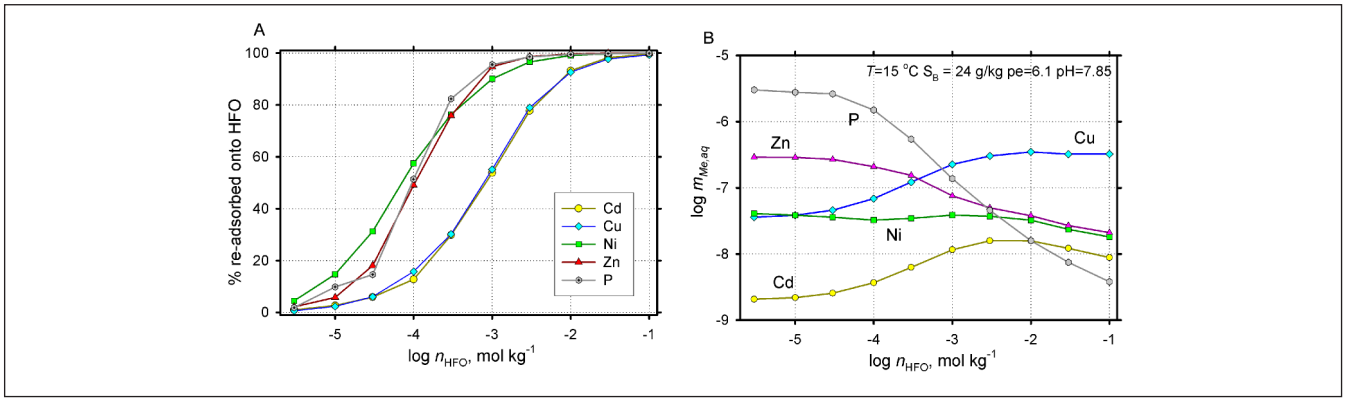

Fig. 3: Modelled scenario of trace metal re-partitioning upon complete 'dissolution' of the HMO phase (at initial n_{HMO} = 270 and X_{HMO} = 0.9) at varying the amounts of HFO n_{HFO} between 30 µM and 0.1 M: (A) re-adsorbed onto the HFO surface, (B) remaining in the Baltic Sea normative water at equilibrium with adsorption on HFO

metal pool, should decrease because of dilution out into the near-bottom water. We assumed that 2/3 of dissolved Mn, Zn, Ni, and Cu diffuse out of the fluffy layer, and that the effective HFO concentration increases with time (which implies local absence of significant water movement at least in the fluffy layer during stagnation). Such a model could reproduce re-adsorption of heavy metals in the extreme case when all HMO gets re-dissolved in a stagnant fluffy layer. Results of 10 model runs for varying amounts of HFO between 30 µM and 0.1 M are shown in **Fig 3**. Heavy metals thus released appear not to be effectively re-adsorbed on the HFO because of strong competition with the dominant pool of adsorbed Mn^{+2}. Only the phosphate oxyanion gets strongly adsorbed, but Cu and Cd remain strongly complexed in the aqueous phase. In the case when the HFO continues precipitating in the stagnant fluffy layer due to release from anoxic sediments, re-adsorption of Zn and Ni may be stronger to an extent depending on the rate of additional supply of dissolved Fe(II), which, however, is usually limited by the solubility of ferrous sulfide phases.

The process of gradual development of stagnation could influence heavy metal partitioning even when HMO is still stable. Complex processes related to heavy metal adsorption on that oxide phase in relation to redox conditions are yet unknown. The present thermodynamic model can give some insight onto what can happen along gradual reduction of the near-bottom water system including ferromanganese nodule. The same system as in previous run, with initial concentration of Fe+Mn = 300 µM and X_{HMO} = 0.9, was therefore run as an equilibrium redox profile. **Fig. 4** shows complex changes in the closed system which would occur upon mineralization of increasing quantities of organic matter (monitored by total dissolved CO_2, C_T). Abrupt changes occur when first HMO and then HFO dissolve completely. The pH first decreases due to addition of CO_2, then increases because of the alkalinity gain by dissolution of the Mn oxide, the latter also changes its O/Mn ratio from 1.9 to 1.5. We assumed that the fraction of the total HMO surface under ion exchange sites X (maximum 30%) decreased in this process proportional to a decrease in the MnO_2 end-member mole fraction of the HMO solid-solution phase. The complex effects of competing metal adsorption are evident in **Fig. 5**. All metals except Zn tend to leave the HMO phase during early stages of reduction, and remain in aqueous solution to the extent of more than 50%. The net effect on aqueous metal concentrations is seen in **Fig. 6**, where weakly adsorbed Cd and Cu increase uniformly, while Zn can be affected by a relatively strong re-adsorption onto HFO after complete dissolution of the Mn oxide, and strong release only upon ultimate dissolution of HFO.

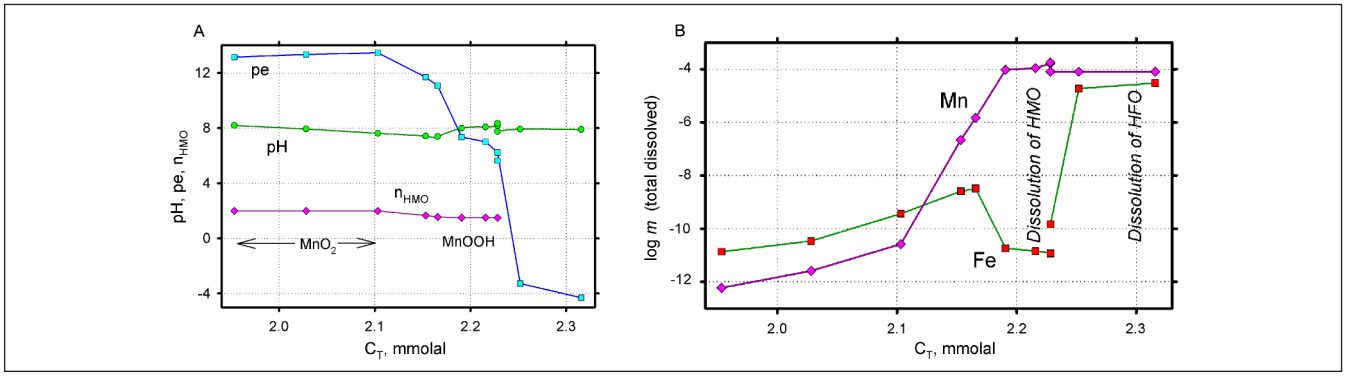

Fig. 4: Effects of gradual development of anoxia: (A) on pe, pH, and HMO oxidation number, and (B) on total dissolved Mn and Fe concentrations upon gradual development of anoxia, simulated by titration of Baltic normative water with the 'organic carbon' C_T in the closed system with n_{HFO} = 30 µM and n_{HMO} = 270 µM (X_{HMO} = 0.9). Note that pH first decreases due to the build-up of dissolved carbonic acid species and then increases because of increasing concentrations of dissolved ammonia from 'organic carbon' as well as dissolved Mn

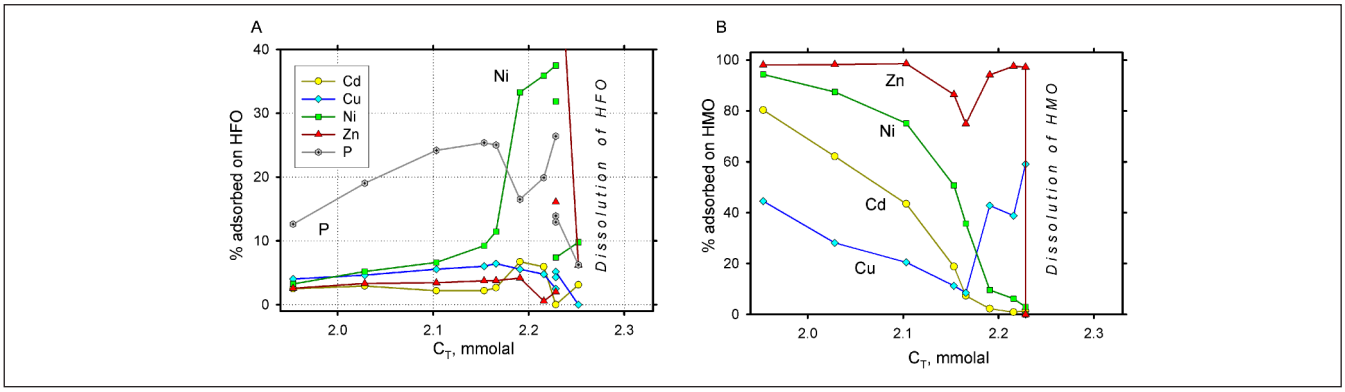

Fig. 5: Simulated effects of gradual development of anoxia on trace element adsorption (A) onto HFO and (B) onto HMO upon reductive dissolution simulated by the C_T (organic carbon) titration in the same closed system as on Fig. 4. Increase of adsorbed Ni on HFO (plot A) should be attributed to pH increase at suboxic part of the redox profile

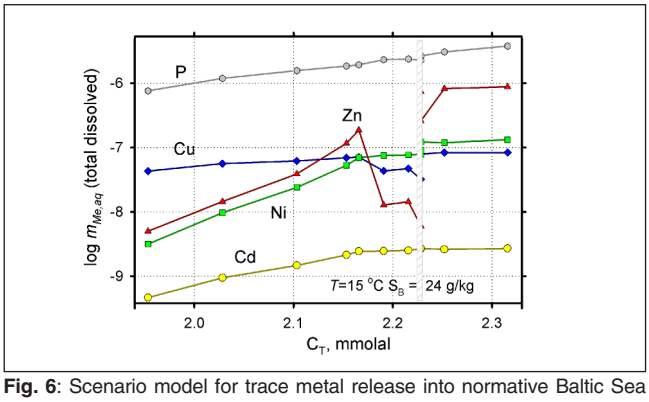

Fig. 6: Scenario model for trace metal release into normative Baltic Sea water upon reductive dissolution of both HMO and HFO, as simulated by the C_T (organic carbon) titration in the same closed system as on Fig. 4. The slashed bar indicates a position of major redox transition where the complete dissolution of HMO and then HFO phases takes place

3 Conclusion and Outlook

Our model accounts qualitatively for a very complex interplay of aqueous and surface speciation, solid carrier solubility, and redox changes. It is preliminary in a sense that the full set of thermodynamic data on the complex microbe-mediated redox behavior of phyllomanganates are still not available. Moreover, one should keep in mind that a complete early-diagenetic model description involves at least additional considering of steady-state pore water diffusion or even non-steady-state turbulent mass transport. The available field data permit at least to formulate a local/partial equilibrium approach which can provide useful boundary conditions which govern partitioning of heavy metals between growing Mn/Fe-accumulate, and aqueous solution in the fluffy layer or near-bottom water body. Our model demonstrates a by far stronger net retention of Zn compared to other metals, and suggests that significant fraction of Mn (and Ni, Cd), probably 50% or more, may be recycled to water column from surface of ferromanganese nodules during stagnation episodes. The model also do not account for reductive dissolution kinetics of HMO and HFO, but many empirical observations suggest that dissolution is relatively fast for Mn oxides due to microbial mediation. Further experimental sorption studies on HMO should focus on (i) low surface coverage, (ii) competition between adsorbed Mn^{+2} and Me^{+n}, and (iii) impact of redox conditions onto composition and surface properties. However, being parameterized by experimental data on solubility and oxidation numbers of synthetic Mn oxides at different redox conditions and pH, the Gibbs energy minimization modeling approach seems to be capable to account for these complex chemical interactions relevant to the Mn/Fe accumulating environment in the Baltic Sea. Such models, even if only first approximations, clearly support the idea that stagnation in the bottom water, once occurring, can drastically change primary element proxy records in ferromanganese nodules. Therefore, one cannot expect that any element peaks in profiles perpendicular to the growth direction, even if measured on a sub-millimetre scale, reflect anything meaningful about original pollutant deposition. Since larger part of the metal pollutant together with the Mn inventory is recycling into the near-bottom water upon stagnation, a strong hysteresis effect must be expected in the thus affected part of the record. Even if any anthropogenic metal supply into the Baltic would be drastically changed from one year to the other, we may not see it in the crust profile before a decade or so later.

Acknowledgements. The authors are pleased to submit this paper in recognition of the distinguished research career of Ulrich Förstner on the occasion of his 65th birthday. Michael Kersten acknowledges the guidance of Professor Förstner as one of his former students, and his encouragement to do not only applied research but also fundamental work in environmental geochemistry.

References

Appelo CAJ, Postma D (1999): A consistent model for surface complexation on birnessite (δ-MnO_2) and its application to a column experiment. Geochim Cosmochim Acta 63, 3039–3048

Bochatay L, Persson P (2000): Metal ion coordination at the water-manganite (γ-MnOOH) interface II. An EXAFS study of zinc(II). J Colloid Interf Sci 229, 593–599

Brown PL, Sylva RN, Ellis J (1985): An equation for predicting the formation constants of hydroxo-metal complexes. J Chem Soc Dalton Trans 85, 723–730

Catts JG, Langmuir D (1986): Adsorption of Cu, Pb and Zn by δ-MnO_2: Applicability of the site binding-surface complexation model. Appl Geochem 1, 255–264

Dzombak DA, Morel FMM (1990): Surface complexation modeling – Hydrous ferric oxides. Wiley Interscience, New York, 331 pp

Fortin D, Leppard GG, Tessier A (1993): Characteristics of lacustrine diagenetic iron oxyhydroxides. Geochim Cosmochim Acta 57, 4391–4404

Giovanoli R, Bürki P, Giuffredi M, Stumm W (1975): Layer structured manganese oxide hydroxides IV. Buserite group: Structure stabilization by transition elements. Chimia 29, 517–520

Glasby GP, Emelyanov EM, Zhamoida VA, Baturin GN, Leipe T, Bahlo R, Bonacker P (1997): Environment of formation of ferromanganese concretions in the Baltic Sea: a critical review. In: Nicholson K, Hein JR, Bühn B, Dasgupta S (eds), Manganese Mineralization: Geochemistry and Mineralogy of Terrestrial and Marine Deposits. Geol Soc Spec Publ 119, 213–237

Gramm-Osipov LM, Tistchenko PY, Stastchuk MF, Volkova TI, Chichkin RV, Shulga YM (1989): Ferro-manganese system. In: Illichev VI (ed), Chemistry of seawater and authigenic mineral formation. Nauka Publ., Moscow, 112–203 (in Russian)

Gramm-Osipov LM, Volkova TI, Chichkin RV (1992): Laboratory data on the behaviour of manganese dioxide in aqueous solution. Geochem Internat 7, 28–36

Harms A (1996): Die bodennahe Trübezone der Mecklenburger Bucht unter besonderer Betrachtung der Stoffdynamik bei Schwermetallen. IOW Marine Science Reports No. 20, 96 pp

Hlawatsch S, Garbe-Schönberg C-D, Lechtenberg F, Manceau A, Tamura N, Kulik DA, Kersten M (2002a): Trace metal fluxes to ferromanganese nodules from the western Baltic Sea as a record for long-term environmental changes. Chem Geol 182, 697–709

Hlawatsch S, Neumann T, van den Berg CMG, Kersten M, Harff J, Suess E (2002b): Fast-growing, shallow-water ferro-manganese nodules from the western Baltic Sea: origin and modes of trace element incorporation. Mar Geol 182, 373–387

Karpov IK, Chudnenko KV, Kulik DA (1997): Modeling chemical mass-transfer in geochemical processes: Thermodynamic relations, conditions of equilibria and numerical algorithms. Am J Sci 297, 767–806

Kersten M, Kulik DA (2005): Thermodynamic modeling of trace element partitioning in the environment: New concepts and outlook. In: Cornelis R, Caruso J, Crews H, Heumann K (eds), Handbook of Elemental Speciation, Vol 2. Wiley & Sons, Chichester, pp 651–689

Kulik DA, Harff J (1993): Physicochemical modeling of the Baltic Sea water system. IOW Marine Science Reports No. 6, 80 pp

Kulik DA, Kersten M (1998): Thermodynamic modeling of heterogeneous sorption of trace metals onto synthetic and natural non-stoichiometric Mn oxides. Mineral Mag 62A, 826–827

Kulik DA (2000): Thermodynamic properties of surface species at the mineral-water interface under hydrothermal conditions: A Gibbs energy minimization single-site $2pK_A$ triple-layer model of rutile in NaCl electrolyte to 250°C. Geochim Cosmochim Acta 64, 3161–3179

Kulik DA (2002a): Gibbs energy minimization approach to modeling sorption equilibria at the mineral-water interface: Thermodynamic relations for multi-site surface complexation. Am J Sci 302, 227–279

Kulik DA (2002b): Sorption modeling by Gibbs energy minimization: Towards a uniform thermodynamic database for surface complexes of radionuclides. Radiochim Acta 90, 815–832

Kulik DA, Kersten M, Heiser U, Neumann T (2000): Application of Gibbs energy minimization to model early-diagenetic solid-solution aqueous-solution equilibria involving authigenic rhodochrosites in anoxic Baltic Sea sediments. Aquatic Geochemistry 6, 147–199

Manceau A, Lanson B, Drits V (2002): Structure of heavy metal sorbed birnessite. Part 3: Results from powder and polarized EXAFS spectroscopy. Geochim Cosmochim Acta 66, 2639–2663

Marcus MA, Manceau A, Kersten M (2004): Mn, Fe, Zn and As speciation in a fast-growing ferromanganese marine nodule. Geochim Cosmochim Acta 68, 3125–3136

Melnik YP (1986): Physicochemical conditions of the origin of Precambrian banded iron formation. Naukova Dumka, Kiev, 260 pp (in Russian)

Müller B, Duffek A (2001): Similar Adsorption Parameters for Trace Metals with Different Aquatic Particles. Aquat Geochem 7, 107–126

Shock EL, Sassani DC, Willis M, Sverjensky DA (1997): Inorganic species in geologic fluids: Correlations among standard molal thermodynamic properties of aqueous ions and hydroxide complexes. Geochim Cosmochim Acta 61, 907–950

Smith RW, Jenne EA (1991): Recalculation, evaluation, and prediction of surface complexation constants for metal adsorption on iron and manganese oxides. Environ Sci Technol 25, 525–531

Sverjensky DA, Sahai N (1997): Theoretical prediction of single-site surface-protonation equilibrium constants for oxides and silicates in water. Geochim Cosmochim Acta 60, 3773–3797

Sverjensky DA, Shock EL, Helgeson HC (1997): Prediction of the thermodynamic properties of aqueous metal complexes to 1000°C and 5 kb. Geochim Cosmochim Acta 61, 1359–1412

Tanaka Y, Tsuji M (1997): Thermodynamic study of alkali metal ion exchange on a manganese dioxide with hexagonal structure. Mat Res Bull 32, 461–475

Tessier A, Fortin D, Belzile N, DeVitre RR, Leppard GG (1996): Metal sorption to diagenetic iron and manganese oxyhydroxides and associated organic matter: Narrowing the gap between field and laboratory measurements. Geochim Cosmochim Acta 60, 387–404

Tonkin JW, Balistrieri LS, Murray JW (2004): Modeling sorption of divalent metal cations on hydrous manganese oxide using the diffuse double layer model. Appl Geochem 19, 29–53

Trivedi P, Axe L, Tyson TA (2001): XAS studies of Ni and Zn sorbed to hydrous manganese oxide. Environ Sci Technol 35, 4515–4521

Tye FL (1985): Manganese dioxide electrode-X. A theoretical treatment based on the concept of two solid solutions in the range γ-MnO_2 to δ-MnOOH. Electrochim Acta 30, 17–23

Received: November 17th, 2004
Accepted: February 2nd, 2005
OnlineFirst: February 3rd, 2005